We are IntechOpen, the world's leading publisher of Open Access books Built by scientists, for scientists

4,800
Open access books available

122,000
International authors and editors

135M
Downloads

Our authors are among the

154
Countries delivered to

TOP 1%
most cited scientists

12.2%
Contributors from top 500 universities

CLARIVATE ANALYTICS BOOK CITATION INDEX INDEXED

WEB OF SCIENCE™

Selection of our books indexed in the Book Citation Index in Web of Science™ Core Collection (BKCI)

Interested in publishing with us?
Contact book.department@intechopen.com

Numbers displayed above are based on latest data collected.
For more information visit www.intechopen.com

5

Quantum Electrodynamics in Photonic Crystal Nanocavities towards Quantum Information Processing

Yun-Feng Xiao[1,2], Xu-Bo Zou[3], Qihuang Gong[1],
Guang-Can Guo[3], and Chee Wei Wong[2]
[1]*State Key Lab for Artificial Microstructure and Mesoscopic Physics, School of Physics, Peking University, Beijing 100871,*
[2]*Optical Nanostructures Laboratory, Center for Integrated Science and Engineering, Solid-State Science and Engineering, and Department of Mechanical Engineering, Columbia University, New York, NY 10027,*
[3]*Key Laboratory of Quantum Information, University of Science and Technology of China, Hefei 230026,*
[1,3]*People's Republic of China*
[2]*USA*

1. Introduction

Cavity quantum electrodynamics (cavity QED) describes few atoms coupling to quantized electromagnetic fields inside an optical cavity (Mabuchi & Doherty, 2002). The core of cavity QED is the strong coherent interaction between the single-mode electromagnetic field and the internal states of the atom. It is one of few experimentally realizable systems in which the intrinsic quantum mechanical coupling dominates losses that due to dissipation (Cirac et al., 1997). Furthermore, it represents an almost ideal and the simplest quantum system which allows quantitative studying of a dynamical open quantum system under continuous observation. Up to the present, three representative optical microcavities have been proposed for studying quantum optics and implementing quantum information (Vahala, 2004). The first one is the conventional Fabre-Perot (FP) type cavities consisting of two concave dielectric mirrors facing each other at a distance of the order of a few 100 μm, where single neutral atoms can be trapped through magneto-optical trap (MOT), optical dipole trap or magnetic trap for a long time (up to several seconds). The second is the microcavities supporting whispering gallery modes, including microspheres, microdisks, and microtoroids. The third type is the nanoscale cavities in photonic crystal (Foresi et al., 1997).
With FP-type microcavities, numerous theoretical schemes have been suggested for generating nonclassical states of cavity fields (Vogel et al., 1993; Parkins et al., 1993; Law et al., 1996) and entangled states of many atoms (Cabrillo et al., 1999), and realizing two-qubit logic gates (Pellizzari et al., 1995; Pachos and Walther, 2002) and universal gates for Fock-state qubits (Santos, 2005), which lead to experimental realization of the Einstein-Podolsky-Rosen (EPR) state of two atoms, Greenberger-Horne-Zeilinger (GHZ) states of three parties

Source: Recent Optical and Photonic Technologies, Book edited by: Ki Young Kim,
ISBN 978-953-7619-71-8, pp. 450, January 2010, INTECH, Croatia, downloaded from SCIYO.COM

(two atoms plus one cavity mode), Schrödinger cat state (Brune et al., 1996), and single-photon state (Brattke et al., 2001) of a cavity field. However, FP-type microcavities have their inherent problems. For example, it is extremely difficult to realize a scalable quantum computation in experiment by integrating many microcavities, though theoretical protocols may be simple and elegant. Recently, whispering gallery microcavities have been studied for cavity QED toward quantum information processing (Xiao et al., 2006) due to their ultrahigh quality factors (Q, which is proportional to the confinement time in units of the optical period) and high physical scalability. Strong-coupling regime has been demonstrated when cold caesium atoms fall through the external evanescent field of a whispering gallery mode. Nevertheless, the cold atoms are ideal stationery qubits (quantum bits), but not suited for good flying qubits. Thus, a solid-state cavity QED (involved single quantum dot (QD), for example) system with whispering gallery microcavities seeks further advancements.

As a new resonant configuration, nanocavities in photonic crystal with high quality factors (Q) and ultrasmall mode volumes (V) are attracting increasing attention in the context of optical cavity QED (Faraon et al., 2008; Fushman et al., 2008; Hennessy et al., 2007; Badolato et al., 2006; Reithmaier et al., 2004; Yoshie et al., 2004). Combined with low loss and strong localization, they present a unique platform for highly integrated nanophotonic circuits on a silicon chip, which can also be regarded as quantum hardware for nanocavity-QED-based quantum computing. Toward this goal, strong interactions between a QD and a single photonic crystal cavity have been observed experimentally (Hennessy et al., 2007; Badolato et al., 2006; Reithmaier et al., 2004; Yoshie et al., 2004). Moreover, single photons from a QD coupled to a source cavity can be remarkably transferred to a target cavity via an integrated waveguide in an InAs/GaAs solid-state system (Englund et al., 2007a), which opens the door to construct the basic building blocks for future chip-based quantum information processing systems. Weak coupling nanocrystal ensemble measurements are reported in TiO2-SiO2 and AlGaAs cavity systems (below 1 μm wavelengths) recently (Guo et al., 2006; Fushman et al., 2005) and also independently in silicon nanocavities with lead chalcogenide nanocrystals (a special kind of QDs) at near 1.55 μm fibre communication wavelengths recently (Bose et al., 2007).

In this Chapter, we theoretically study the coherent interaction between single nanocrystals and nanocavities in photonic crystal. This Chapter is organized as follows. In section 2, our attention is focused on a single QD embedded in a single nanocavity. First, we introduce, derive, and demonstrate the explicit conditions toward realization of a spin-photon phase gate, and propose these interactions as a generalized quantum interface for quantum information processing. Second, we examine single-spin-induced reflections as direct evidence of intrinsic bare and dressed modes in our coupled nanocrystal-cavity system. In section 3, however, our attention is switched on the N coupled cavity-QD subsystems. We examine the spectral character and optical delay brought about by the coupled cavities interacting with single QDs, in an optical analogue to electromagnetically induced transparency (EIT) (Fleischhauer et al., 2005). Furthermore, we then examine the usability of this coupled cavity-QD system for QD-QD quantum phase gate operation and our numerical examples suggest that a two-qubit system with high fidelity and low photon loss.

2. Nanocrystals in silicon photonic crystal standing-wave cavities

In this section, we examine the single-photon pulse (or weak coherent light pulse) interactions of a single semiconductor nanocrystal in a system comprised of standing-wave

high-Q/V silicon photonic crystal nanocavities (Xiao et al., 2007a). In contrast to earlier travelling-wave whispering gallery cavity studies (Xiao et al., 2006), we show here that a QED system based on coupled standing-wave nanocavities can realize a spin-photon phase gate even under the bad-cavity limit and provide a generalized quantum interface for quantum information processing. In addition, we demonstrate numerically a solid-state universal two-qubit phase gate operation with a single qubit rotation. This theoretical study is focused within the parameters of near 1.55 μm wavelength operation for direct integration with the fiber network, and in the silicon materials platform to work with the vast and powerful silicon processing infrastructure for large-array chip-based scalability.

2.1 Theoretical model

We begin by considering a combined system consisting of coupled point-defect high-Q/V photonic crystal cavities, a line-defect photonic crystal waveguide, and an isolated single semiconductor nanocrystal. We offer some brief remarks on this system before building our theoretical model. When a photon pulse is coupled into the cavity mode via a waveguide (Fig. 1(a)), photons can couple out of the cavity along both forward and backward propagating directions of the waveguide because the cavity supports standing-wave modes. While each cavity can each have a Faraday isolator to block the backward propagating photon, such implementation may not be easily scalable to a large-array of cavities. To obtain only forward transmission, here we examine theoretically a defect cavity system with accidental degeneracy (Fan et al., 1998; Xu et al., 2000; Min et al., 2004) as a generalized study of *cavity-dipole-cavity* systems, and which also provides close to 100% forward-only drop efficiency. This framework is also immediately applicable to non-reciprocal magneto-optic cavities which have larger fabrication tolerances. Both systems support two degenerate even $|e\rangle$ and odd $|o\rangle$ cavity modes (*h*-polarized, dominant in-plane *E*-field) that have opposite parity due to the mirror symmetry, as shown in Fig. 1(a). The waveguides can support both *v*-polarizations (dominant in-plane *H*-field) and *h*-polarizations for polarization diversity (Barwicz et al., 2007).

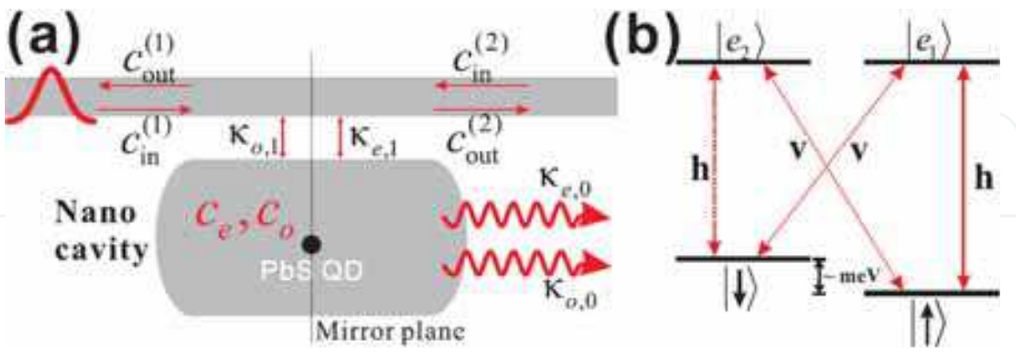

Fig. 1. (a) Sketch of a waveguide side coupled to a cavity which supports two degenerate modes c_e and c_o with opposite parity. (b) lead chalcogenide (e.g. lead sulphide) nanocrystal energy levels and the electron-exciton transitions in the presence of a strong magnetic field along the waveguide direction, which produces nondegenerate transitions from the electron spin states $|\uparrow\rangle$ and $|\downarrow\rangle$ to the charged exciton states $|e_1\rangle$ and $|e_2\rangle$ under the transition selection rules.

Fig. 1(b) shows the energy levels and electron-exciton transitions of our cavity-dipole-cavity system. In order to produce nondegenerate transitions from the electron spin states, a magnetic field is applied along the waveguide direction (Atatüre et al., 2006). $|\uparrow\rangle$ and $|\downarrow\rangle$ play the rule of a stationary qubit, which have shown much longer coherence time than an exciton (dipole or charge). The transition $\left|\uparrow\right\rangle \leftrightarrow \left|e_1\right\rangle$, with the descending operator $\sigma_- = \left|\uparrow\right\rangle\left\langle e_1\right|$, is especially chosen and coupled with the cavity modes with single-photon coupling strengths $g_e(\vec{r})$ and $g_o(\vec{r})$, while other transitions are decoupled with the cavity modes.

Now we construct our model by studying the interaction between the nanocrystal and the cavity modes. The Heisenberg equations of motion for the internal cavity fields and the nanocrystal are (Duan et al., 2003; Duan & Kimble et al., 2004; Sørensen & Mølmer, 2003)

$$\frac{dc_e}{dt} = -\mathrm{i}\left[c_e, H\right] - \kappa_e c_e + \mathrm{i}\sum_{j=1,2}\sqrt{\kappa_{e1}}c_{\mathrm{in}}^{(j)}, \tag{1}$$

$$\frac{dc_o}{dt} = -\mathrm{i}\left[c_o, H\right] - \kappa_o c_o + (-1)^{j+1}\sum_{j=1,2}\sqrt{\kappa_{o1}}c_{\mathrm{in}}^{(j)}, \tag{2}$$

$$\frac{d\sigma_-}{dt} = -\mathrm{i}\left[\sigma_-, H\right] - \gamma\sigma_-, \tag{3}$$

where the interaction Hamiltonian

$$H = \delta_{al}\sigma_+\sigma_- + \sum_{p=e,o}\left[\delta_{cl}c_p{}^{\dagger}c_p + g_p(\vec{r})c_p\sigma_+ + h.c.\right] \tag{4}$$

is in a rotating frame at the input field frequency ω_l. In contrast to earlier work [Xiao et al., 2006; Waks & Vuckovic, 2004; Srinivasan & Painter, 2007], here we examine the case with the two $|e\rangle$ and $|o\rangle$ modes in the standing-wave cavities in order for forward-only propagation of the qubit. The cavity dissipation mechanism is accounted for by $\kappa_{e(o)} = \kappa_{e(o)0} + \kappa_{e(o)1}$, where $\kappa_{e(o)0}$ is intrinsic loss and $\kappa_{e(o)1}$ the external loss for the even (odd) mode. The nanocrystal dissipation is represented by $\gamma \equiv \gamma_s/2 + \gamma_p$ where γ_s is the spontaneous emission rate and γ_p the dephasing rate of the nanocrystal.

When the two degenerate modes have the same decay rate, i.e., $\kappa_{e0} = \kappa_{o0} = \kappa_0$, $\kappa_{e1} = \kappa_{o1} = \kappa_1$, and $\kappa \equiv \kappa_0 + \kappa_1$, two new states $\left|\pm\right\rangle = \left(\left|e\right\rangle \pm \mathrm{i}\left|o\right\rangle\right)/\sqrt{2}$ are suitable to describe this system, which can be thought as two traveling (or rotating) modes. In this regard, the interaction Hamiltonian is expressed as

$$H = \delta_{al}\sigma_+\sigma_- + \sum_{s=+,-}\left[\delta_{cl}c_s{}^{\dagger}c_s + g_s(\vec{r})c_s\sigma_+ + h.c.\right] \tag{5}$$

where the effective single-photon coupling rates are $g_{\pm}(\vec{r}) = \left(g_e(\vec{r}) \mp \mathrm{i}g_o(\vec{r})\right)/\sqrt{2}$. In this case, Eqs. (1) , (2), and (3) are rewritten into the corresponding forms with $c_{\pm}$.

The nanocrystal-cavity system is excited by a weak monochromatic field (e.g., single-photon pulse), so that we solve the above motion equations for the below explicit analytical expressions

$$\sigma_-(\omega) = -\mathrm{i}\sum_{s=+,-} g_s(\vec{r})c_s(\omega)/\left(\mathrm{i}\delta_{al} + \gamma\right) \tag{6}$$

and $c_{\pm}(\omega)$ are given as

$$\mathrm{i}\sqrt{2\kappa_1}c_{\mathrm{in}}^{(1)}(\omega)-(\mathrm{i}\delta_{cl}+\kappa)c_{+}(\omega)-\mathrm{i}g_{+}^{*}(\vec{r})\sigma_{-}(\omega)=0\,, \tag{7}$$

$$\mathrm{i}\sqrt{2\kappa_1}c_{\mathrm{in}}^{(2)}(\omega)-(\mathrm{i}\delta_{cl}+\kappa)c_{-}(\omega)-\mathrm{i}g_{-}^{*}(\vec{r})\sigma_{-}(\omega)=0\,. \tag{8}$$

Note that orthogonality of the $|e\rangle$ and $|o\rangle$ basis modes (as shown in Fig. 1a) forces the nanocrystal to choose only either $g_e(\vec{r})=ig_o(\vec{r})$, or $g_e(\vec{r})=-ig_o(\vec{r})$, or both (in which case $|e\rangle$ and $|o\rangle$ are uniquely zero), but no other possibilities. Photon qubit input from only the left waveguide forces only one of the cavity states ($|e\rangle + \mathrm{i}|o\rangle$) to exist (Fan et al., 1998), and we assume this cavity environment from the existing photon qubit enhances the $g_e(\vec{r})=-ig_o(\vec{r})$ probability. Of course, with only the left waveguide qubit input in a non-reciprocal magneto-optic cavity, this condition is strictly enforced. Hence we can take $g_e(\vec{r})=-\mathrm{i}g_o(\vec{r})$, which implies $g_{-}(\vec{r})=0$, $g_{+}(\vec{r})=\sqrt{2}g_e(\vec{r})$, to further simplify Eqs. (7)-(8). Now note that the left output $c_{\mathrm{out}}^{(1)}$ remarkably vanishes, while the right output is given by $c_{\mathrm{out}}^{(2)}=c_{\mathrm{in}}^{(1)}(\kappa-2\kappa_1-\mathrm{i}\delta+\lambda)/(\kappa-\mathrm{i}\delta+\lambda)$, where $\lambda=2|g_e(\vec{r})|^2/[\mathrm{i}(\Delta-\delta)+\gamma]$, and $\Delta\equiv\delta_{al}-\delta_{cl}$ and $\delta\equiv-\delta_{cl}$ denote the nanocrystal-cavity and input-cavity detunings, respectively. Importantly, this implies that our quantum phase gate provides a *true* one-way transmission through the cavity-dipole-cavity system.

2.2 Spin-photon phase gate

To examine more of the underlying physics, we consider first the case of exact resonance ($\Delta=0$, $\delta=0$). When $g_e(\vec{r})|^2/\kappa\gamma>>1$ (the nanocrystal occupies the spin state $|\uparrow\rangle$), we obtain $c_{\mathrm{out}}^{(2)}\approx c_{\mathrm{in}}^{(1)}$. When $g_e(\vec{r})=0$ (the nanocrystal occupies the spin state $|\downarrow\rangle$), we obtain $c_{\mathrm{out}}^{(2)}\approx -c_{\mathrm{in}}^{(1)}$ for $\kappa_1>>\kappa_0$, which indicates that the system achieves a *global* phase change $e^{\mathrm{i}\pi}$. This distinct characteristic allows the implementation of a spin-photon phase gate. After the photon pulse passes though the cavity system, we easily obtain a gate operation

$$\begin{aligned}&|h\rangle|\uparrow\rangle\rightarrow|h\rangle|\uparrow\rangle,\ |h\rangle|\downarrow\rangle\rightarrow-|h\rangle|\downarrow\rangle,\\&|v\rangle|\uparrow\rangle\rightarrow|v\rangle|\uparrow\rangle,\ |v\rangle|\downarrow\rangle\rightarrow|v\rangle|\downarrow\rangle.\end{aligned} \tag{9}$$

This two-qubit phase gate combined with simple single-bit rotation is, in fact, universal for quantum computing. More importantly, this interacting system can be regarded as a quantum interface for quantum state sending, transferring, receiving, swapping, and processing.

To efficiently evaluate the quality of the gate operation, the gate fidelity is numerically calculated, as shown in Fig. 2. Considering specifically a lead chalcogenide (e.g. lead sulphide) nanocrystal and silicon photonic nanocavity system for experimental realization, we choose the spontaneous decay as γ_s ~ 2 MHz and all non-radiative dephasing γ_p ~ 1 GHz at cooled temperatures. Photonic crystal cavities have an ultrasmall mode volume V (~ 0.1 μm^3 at 1550 nm), with a resulting calculated single-photon coherent coupling rate $|g_e|$ of ~ 30 GHz. High Q of up to even ~10^6 experimentally and ~10^7 theoretically (Asano et al., 2006; Kuramochi et al., 2006) has been achieved in photonic crystal cavities.

With these parameters, as shown in Fig. 2a, the gate fidelity of the cavity-dipole-cavity system can reach 0.98 or more, even when photon loss is taken into account, and even when

the vacuum Rabi frequency g_e is lower than the cavity decay rate κ (bad-cavity limit). The gate fidelity increases initially as the cavity approaches more into the over-coupling regime due to less photon loss and eventually decreases as the nanocrystal-cavity system moves away from the strong coupling regime. Secondly, we note that with non-zero detuning (Δ/κ_o=2; Case III and VI), the gate fidelity slightly decreases but is still adequate. With increasing nanocrystal dissipation rate (Fig. 2b), the fidelity decreases as expected and the system moves away from strong coupling (less nanocrystal interactions with the cavity). The physical essence behind such high fidelities is the true one-way transmission where the nanocrystal couples to $|+\rangle$ mode, with only forward propagation with no backward scattering of the qubit. In addition, accidental degeneracy mismatch may degrade the gate performance. To validate the feasibility of the present scheme, we perform a direct calculation of gate fidelity for different frequency and lifetime of the opposite-parity cavity modes. Even with degeneracy mismatch (ω_e - ω_l = $\delta_{el} \neq \delta_{ol}$ = ω_o - ω_l; in Case IV and VII) with some backward scattering of the qubit, the gate fidelity is shown to remain high. Moreover, with different lifetimes of the cavity modes (Case VII), the fidelity remains high as long as the $|g(\vec{r})|^2/\kappa\gamma >> 1$ condition is satisfied.

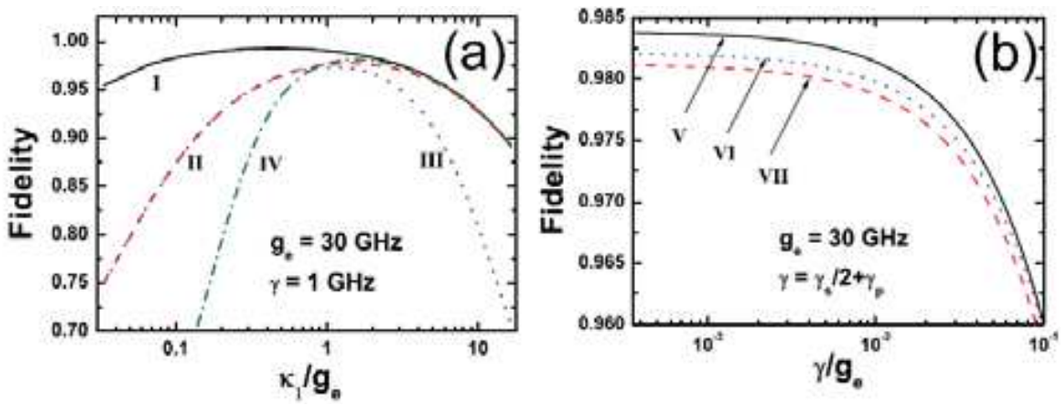

Fig. 2. Gate fidelity versus κ_1 (panel a) and γ (panel b) respectively for the lead sulphide nanocrystal in degenerate cavity modes, illustrating that the fidelity mainly depends on $g_e^2/\kappa\gamma$ and κ_0/κ_1. **Case I:** κ_0 = 0.1 GHz, δ_{el} = δ_{ol} = δ_{al} = 0. **Case II:** κ_0 = 1GHz, δ_{el} = δ_{ol} = δ_{al} = 0. **Case III:** κ_0 = 1GHz, δ_{el} = δ_{ol} = 0, δ_{al} = 5κ_0. **Case IV:** κ_{e0} = κ_{o0} = 0.1GHz, δ_{el} = -δ_{ol} = 5GHz, δ_{al} = 0. **Case V:** κ_{e0} = κ_{o0} = κ_0 = 1GHz, κ_{e1} = κ_{o1} = κ_1 = g_e, δ_{el} = δ_{ol} = δ_{al} = 0. **Case VI:** identical to Case V but with δ_{al} = 5κ_0. **Case VII:** κ_{e0} = 2κ_{o0} = 0.2GHz, κ_{e1} = 1.1κ_{o1} = g_e, δ_{el} = -δ_{ol} = 5GHz, δ_{al} = 1GHz.

2.3 Single-spin-induced reflections

Furthermore, we show that the above cavity-dipole-cavity interaction mechanism can result in interesting transmissions and reflections based on the presence or absence of dipole interaction, and with different detunings. We examine the case of $g_e(\vec{r}) = g$ and $g_o(\vec{r}) = 0$, such as when the nanocrystal is positioned at the cavity mirror plane. Some typical transmission and reflection spectra are shown in Fig. 3. In the absence of a dipole (i.e., the nanocrystal occupies the spin state $|\downarrow\rangle$), the cavity system has near-unity transmission, except when on-resonance. However, when the located nanocrystal is in state $|\uparrow\rangle$, the interacting system is transmission-free and remarkably reflects the cavity field strongly. We

emphasize that this reflection is induced by a *single* spin state, and hence can be termed single-spin-induced reflection. The constructive interference of the cavity field can be considered as an optical-analog to electromagnetically induced absorption in the excited state of a 3-level atomic system. The three reflection peaks in Fig. 3(a) can be understood by considering the strong cavity-dipole-cavity interaction, where the input photon pulse experiences three modes: bare odd mode (central peak) and two dressed even modes (side peaks). When the total cavity decay increases, the three peaks overlap increasingly and form a new peak (Figs. 3b-3d) at zero detuning input. We note the high reflectivity for the cavity-dipole-cavity system at zero detuning, even under the bad-cavity limit. This high reflectivity is helpful to permit arrayed controlled phase flip operation with a single circulator at the input.

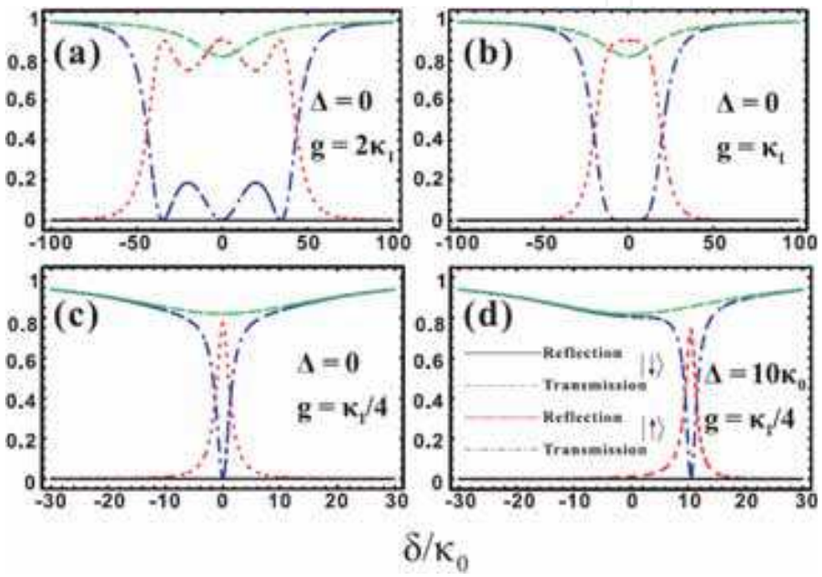

Fig. 3. Reflection and transmission of the spin-photon phase gate with an isolated semiconductor nanocrystal in the degenerate point-defect standing-wave cavity modes. Other conditions for this parameter set include: $\gamma = \kappa_0 / 10$ and $\kappa_1 = 20\kappa_0$, with the nanocrystal located at the cavity mirror plane ($g_e(\vec{r}) = g$ and $g_o(\vec{r}) = 0$). The black solid (green dashed) line is the reflection (transmission) in the absence of a dipole in the cavity. The red dotted (blue dashed-dot) line is the reflection (transmission) in the presence of a dipole in the cavity.

3. Coupled electrodynamics in photonic crystal cavities

Over the past few years, theoretical and experimental interests are mainly focused on a single cavity interacting with atoms, and tremendous successes have been made ranging from strongly trapping single atoms and deterministic generation of single-photon states, to observation of atom-photon quantum entanglement and implementation of quantum communication protocols. For more applications, current interest also lies in the coherent interaction among distant cavities. The coherent interaction of cavity arrays has been studied as an optical analogue to EIT in both theory (Smith et al., 2004; Xiao et al., 2007b) and experiment (Xu et al., 2006; Totsuka et al., 2007). Coupled cavities can be utilized for coherent optical information storage because they provide almost lossless guiding and

coupling of light pulses at slow group velocities. When dopants such as atoms or QDs interact with these cavities, the spatially separated cavities have been proposed for implementing quantum logic and constructing quantum networks. Recent studies also show a strong photon-blockade regime and photonic Mott insulator state (Hartmann et al., 2006; Hartmann & Plenio, 2007), where the two-dimensional hybrid system undergoes a characteristic Mott insulator to superfluid quantum phase transition at zero temperature (Greentree et al., 2006; Angelakis et al., 2007). Recently, it has shown that coupled cavities can also model an anisotropic Heisenberg spin-1/2 lattice in an external magnetic field (Hartmann et al., 2007). The character of a coupled cavity configuration has also been studied using the photon Green function (Hughes, 2007).

3.1 Model of coupled N cavity–QD subsystems

Using transmission theory, we study coherent interactions in a cavity array that includes *N* cavity–QD subsystems (Xiao et al., 2008), with indirect coupling between adjacent cavities through a waveguide (Fig. 4). First, we investigate a subsystem in which a single cavity interacts with an isolated QD. Here for simplicity we suppose that only a single resonance mode (*h*-polarized) is present in the cavity, although two-mode cavity–QD interactions have been considered in the previous section. The cavity–QD–waveguide subsystem has mirror-plane symmetry, so that the mode is even with respect to the mirror plane. We can easily obtain the Heisenberg equations of motion

$$\frac{d\hat{c}_j}{dt} = -i\left[\hat{c}_j, H_j\right] - \Gamma_j \hat{c}_j + i\sqrt{\kappa_{1,j}}\left(\hat{a}_{\mathbf{in}}^{(\mathbf{j})} + \hat{b}_{\mathbf{in}}^{(\mathbf{j})}\right) \tag{10}$$

$$\frac{d\hat{\sigma}_{-,j}}{dt} = -i\left[\hat{\sigma}_{-,j}, H_j\right] - \gamma_j \hat{\sigma}_{-,j} + \sqrt{\gamma_j'}\hat{\sigma}_j' \tag{11}$$

where c_j is bosonic annihilation operator of the *j*-th cavity mode with resonant frequency $\omega_{c,j}$. $\hat{a}_{\mathbf{in}}^{(\mathbf{j})}(\hat{b}_{\mathbf{in}}^{(\mathbf{j})})$ and $\hat{a}_{\mathbf{out}}^{(\mathbf{j})}(\hat{b}_{\mathbf{out}}^{(\mathbf{j})})$ describe the input and output fields in the left (right) port respectively, with standard input-output relations $\hat{a}_{\mathbf{out}}^{(\mathbf{j})} = \hat{b}_{\mathbf{in}}^{(\mathbf{j})} + \sqrt{\kappa_{1,j}}\hat{c}_j$ and $\hat{b}_{\mathbf{out}}^{(\mathbf{j})} = \hat{a}_{\mathbf{in}}^{(\mathbf{j})} + \sqrt{\kappa_{1,j}}\hat{c}_j$. $2\Gamma_j$ represents total cavity decay with $\Gamma_j = \left(\kappa_{0,j} + 2\kappa_{1,j}\right)/2$, where $\kappa_{0,j}$ is the intrinsic cavity decay rate and $\kappa_{1,j}$ the external cavity decay rate. $\hat{\sigma}_{-(+),j}$ is the descending (ascending) operator of the interacting two-level QD with transition frequency $\omega_{r,j}$. γ_j is the total decay rate of the QD, including the spontaneous decay (at rate γ_s) and dephasing (at rate γ_p) in the excited state $|e\rangle$; H_j is the subsystem Hamiltonian $H_j = \omega_{c,j}\hat{c}_j^{\dagger}\hat{c}_j + \omega_{r,j}\hat{\sigma}_{+,j}\hat{\sigma}_{-,j} + \left[g_j(\vec{r})\hat{\sigma}_{+,j}\hat{c}_j + h.c.\right]$, where $g_j(\vec{r})$ is the coupling strength between the cavity mode and the dipolar transition $|g\rangle \leftrightarrow |e\rangle$. $\hat{\sigma}_j'$ is the vacuum noise operator associated with the decay rate γ_j'.

In the weak excitation limit (excited by a weak monochromatic field or a single photon pulse with frequency ω), and by omitting the term which concerns the Langevin noises, the motion equations can be solved, with the transport relation in the frequency domain

$$\begin{pmatrix} \hat{b}_{\text{in}}^{(\text{j})}(\omega) \\ \hat{b}_{\text{out}}^{(\text{j})}(\omega) \end{pmatrix} = T_j \begin{pmatrix} \hat{a}_{\text{in}}^{(\text{j})}(\omega) \\ \hat{a}_{\text{out}}^{(\text{j})}(\omega) \end{pmatrix} \tag{12}$$

Here the transmission matrix is

$$T_j = \frac{1}{\alpha_j + \kappa_{1,j} - \Gamma_j}\begin{pmatrix} -\kappa_{1,j} & \alpha_j - \Gamma_j \\ \alpha_j - \Gamma_j + 2\kappa_{1,j} & \kappa_{1,j} \end{pmatrix} \tag{13}$$

where $\alpha_j = i\Delta_{c,j} + \left|g_j(\vec{r})\right|^2 / \left(i\Delta_{r,j} - \gamma_j\right)$, $\Delta_{c,j} = \omega - \omega_{c,j}$ ($\Delta_{r,j} = \omega - \omega_{r,j}$) represents the detuning between the input field and the cavity mode (QD transition). For convenience, we also define the cavity-QD detuning $\delta_j \equiv \omega_{c,j} - \omega_{r,j}$. The transport matrix can be regarded as a basic cell in cascading subsystems and obtaining the whole transportation for the N-coupled cavity-QD system. The transport properties can thus be expressed as

$$\begin{pmatrix} \hat{b}_{\text{in}}^{(\text{N})}(\omega) \\ \hat{b}_{\text{out}}^{(\text{N})}(\omega) \end{pmatrix} = T_N T_0 \cdots T_0 T_2 T_0 T_1 \begin{pmatrix} \hat{a}_{\text{in}}^{(1)}(\omega) \\ \hat{a}_{\text{out}}^{(1)}(\omega) \end{pmatrix}. \tag{14}$$

Here T_0, the transmission matrix via the waveguide between the two adjacent nanocavities, can be expressed as

$$T_0 = \begin{pmatrix} 0 & e^{-i\theta} \\ e^{i\theta} & 0 \end{pmatrix} \tag{15}$$

where $\theta = \vec{k} \cdot \vec{L}$, and L is the distance between the adjacent nanocavities.

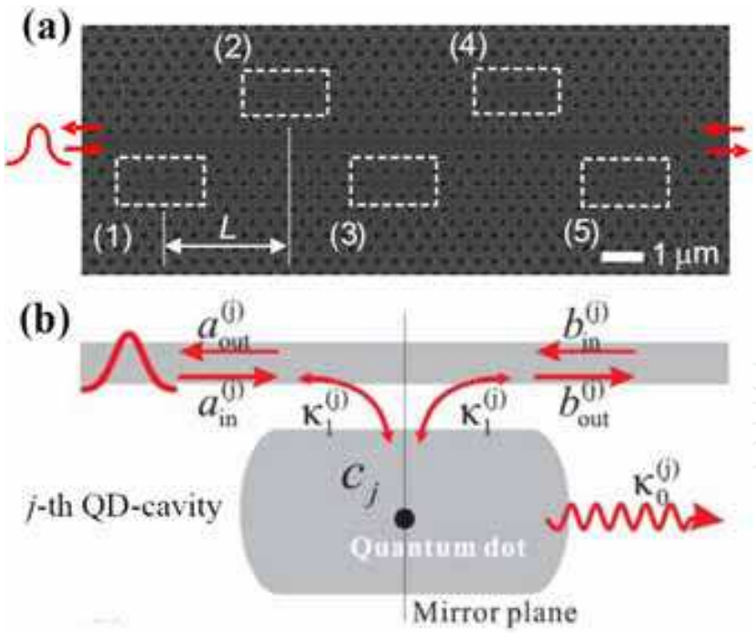

Fig. 4. (a) Example scanning electronic micrograph of periodic waveguide-resonator structure containing N side-coupled nanocavities (h-polarized) at a distance L. The nanocavities are side coupled through the integrated waveguide, with no direct coupling between any two nanocavities. (b) The j-th quantum dot – cavity subsystem. $\hat{a}_{\text{in}}^{(j)}(\hat{b}_{\text{in}}^{(j)})$ and $\hat{a}_{\text{out}}^{(j)}(\hat{b}_{\text{out}}^{(j)})$ describe the input and output fields in the left (right) port, respectively.

When studying only the spectral character of the coupled cavity-QD interaction (Section 3.2), we note that this is analogous to classical microwave circuit design, where the transmission and reflection characteristics from Eq. (14) can also be examined with coupled-mode theory with dipole terms inserted. Examining the spectral character first (Section 3.2) helps to understand the coupled cavity-QD controlled quantum phase gate operation and performance (Sections 3.3 and 3.4).

3.2 Spectral character of coupled cavity-QD arrays

To examine the physical essence, we need to first examine the spectral character of the coupled cavity-QD system. The reflection and transmission coefficients are defined as $r_{N1}(\omega) \equiv \hat{a}^{(1)}_{\mathbf{out}}(\omega) / \hat{a}^{(1)}_{\mathbf{in}}(\omega)$ and $t_{N1}(\omega) \equiv \hat{b}^{(N)}_{\mathbf{out}}(\omega) / \hat{a}^{(1)}_{\mathbf{in}}(\omega)$. In the following, we also assume that these cavities possess the same dissipation characteristic without loss of generality, *i.e.*, $\kappa_{0,j} = \kappa_0$, $\kappa_{1,j} = \kappa_1$, $\kappa_1 = 50\kappa_0$, and $\Gamma_j = \Gamma$.

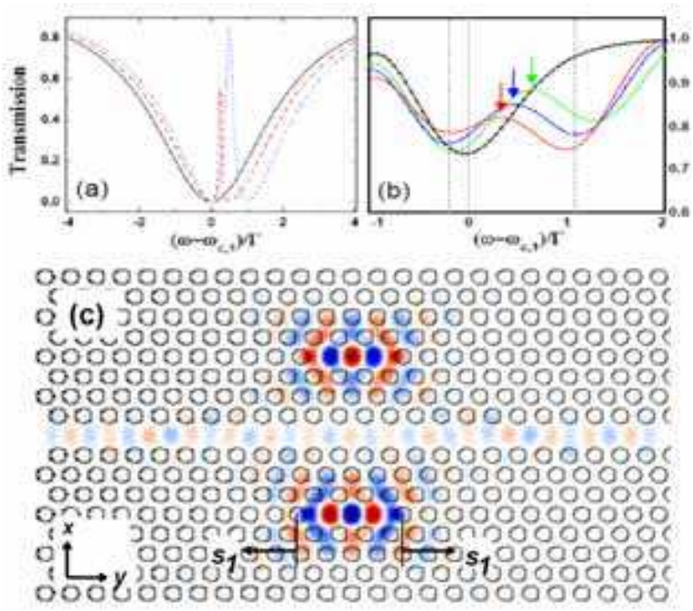

Fig. 5. (a) and (b): Transmission spectra of two coupled empty cavities, where $\theta = 20\pi$. Solid, dashed, and dotted lines describe the cases of $\delta_{21} = 0, \Gamma / 2, \Gamma$, respectively. (b) Numerical 3D FDTD simulations of optical analogue of EIT in two coupled cavity ($\theta = 0$) for detunings 1.14Γ (red; $\Delta\varepsilon_{\mathbf{cavities}} = 0.135$), 1.26Γ (blue; $\Delta\varepsilon_{\mathbf{cavities}} = 0.160$), and 1.49Γ (green; $\Delta\varepsilon_{\mathbf{cavities}} = 0.185$). The arrows denote the EIT peak transmissions. The dashed grey lines denote the two detuned individual resonances for the case of $s_1 = 0.05a$. The black curve is for a single cavity transmission for reference. (c) Example E_x -field distribution of coupled empty photonic crystal cavities.

Fig. 5a describes the transmission spectra of two coupled *empty* cavities (without QD) with different detuning ($\delta_{21} \equiv \omega_{c,2} - \omega_{c,1}$). When the two cavities are exactly resonant, a transmission dip is observed; with increasing δ_{21}, a sharp peak exists at the center position between the two cavity modes. This is an optical analogue to the phenomenon of EIT in atomic vapors. We examine the classical optical analogue exactly through 3D finite-

difference time-domain (FDTD) numerical simulations. Specifically, Fig. 5b and 5c show an example of the transmission and field distributions through the coherent interaction with two coupled *empty* cavities, where the resonance of one cavity is detuned by three cases: $\delta_{21} = 1.14\Gamma$, 1.26Γ , and 1.49Γ . The optical transparency peak from the FDTD is broader than in Fig. 5a due to the finite grid-size resolution, and is observed on top of a background Fabry-Perot oscillation (due to finite reflections at the waveguide facets). The analogy and difference between an all-optical analogue to EIT and atomic EIT are recently discussed in Ref. (Xiao et al., 2007).

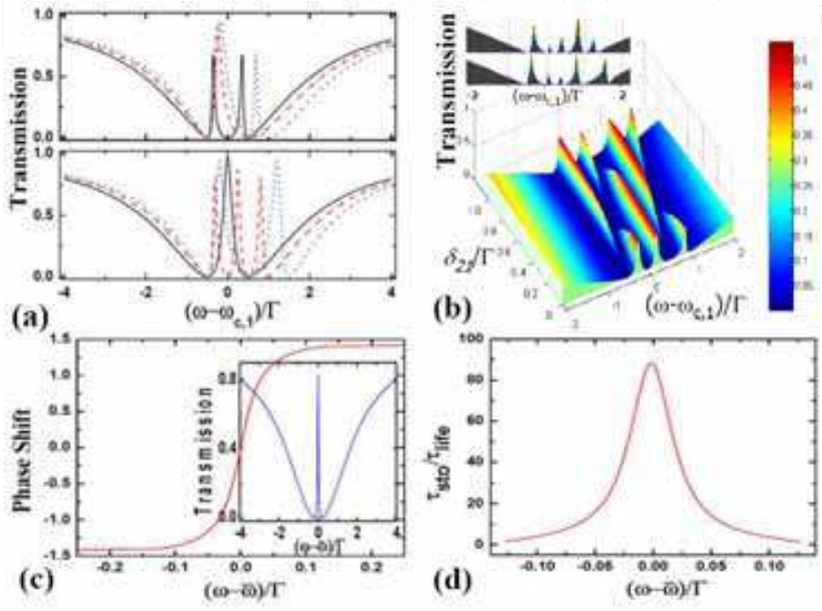

Fig. 6. (a) Transmission spectra of two coupled subsystems with one QD (top) and two QDs (bottom) where $g = \Gamma / 2$, $\gamma = \gamma_1 = \gamma_2 = \kappa_0$. Other conditions are same as Fig. 5a. (b) Spectral character of three coupled subsystems with $\delta_{31} = \Gamma / 2$ and $\delta_{1,2,3} = 0$. Inset: $\delta_{31} = \Gamma / 2$, $\delta_{21} = 0$, $\delta_1 = \delta_3 = 0$, with $\delta_2 = \Gamma / 2$ (top) and Γ (bottom). (c) and (d): Photon phase shift and delay ($\tau_{\mathtt{sto}}$) through two cavity-QD subsystems, where $\omega_{c(r),j} = \varpi$, $g = 0.2\Gamma$. Inset: transmission spectrum.

In the presence of QDs, Fig. 6a (top) shows the spectral characteristics in which a single QD resonantly interacts with the first cavity. When both cavities are resonant, there exist two obvious sharp peaks located symmetrically around $\omega = 0$ (for convenience, we define $\omega_{c,1} = 0$). This fact can be explained by dressed-mode theory. Resonant cavity-QD interaction results in two dressed modes, which are significantly detuned from the second *empty* cavity with the detuning $\pm\left|g_1(\vec{r})\right| = \pm\Gamma / 2$. Both dressed modes non-resonantly couple with the empty mode, resulting in two transparency peaks located at frequencies $\omega \approx \pm\Gamma / 4$. When $\delta_{21} = \Gamma / 2$, one dressed cavity mode non-resonantly couples with the empty mode with a detuning Γ , which leads to a transparency peak located near $\omega \simeq 0$; while the other dressed mode resonantly couples with the empty mode, which does not result in a transparency peak. When δ_{21} continually increases, e.g., $\delta_{21} = \Gamma$, the vanished peak reappears since the two dressed modes are always non-resonant with the empty mode.

Fig. 6a (bottom) illustrates the case where both cavities resonantly interact with a single QD each. Similar to the above analysis, we can explain the number and locations of sharp peaks with respect to different δ_{21} by comparing the two pairs of dressed modes. For example, when $\delta_{21} = \Gamma$, the dressed modes in the first cavity is located at $\pm\Gamma/2$ while the second pair is at $\Gamma/2$ and $3\Gamma/2$, so the transparency peaks are located at $[-\Gamma/2, \Gamma/2]$ and $[\Gamma/2, 3\Gamma/2]$, i.e., two peaks are near 0 and Γ. Fig. 6b shows the spectral character of three coupled cavity-QD subsystems, under various cavity-cavity and cavity-QD detunings. These transmission characteristics are helpful during experimental realization efforts to identify the required tuning and detunings when multiple QD transitions and cavity resonances are involved.

Phase shift and photon storage.– To further examine this coupled cavity-QD system, Fig. 6c shows the transmission phase shift for various detunings of the input photon central frequency, where the cavity and QD transition are resonant for both subsystems. The phase shift has a steep change as we expected intuitively, which corresponds to a strong reduction of the group velocity of the photon. As shown in Fig. 6d, the delay time (τ_{sto}) in this coupled system is almost hundreds of the cavity lifetime ($\tau_{life} = 1/2\Gamma$). This coupled cavity-QD system can essentially be applied to the storage of the photon. Moreover, our solid-state implementation has an achievable bandwidth of ~ 50 MHz in contrast to less than 100 kHz in atomic systems, although the delay-bandwidth product is comparable. To obtain longer photon storage, one can consider dynamical tuning (Yanik et al., 2004; Xu et al., 2007; Yanik & Fan, 2007) to tune the cavity resonances with respect to the QD dipolar transitions to break the delay-bandwidth product in a solid-state cavity-QD array system.

3.3 Quantum phase gate operation

In the section above, we have shown the novel transport character of the coupled cavity-QD system. Now we study the possibility of quantum phase gate operation of the QDs based on this transport character. The schematic to realize this multi-QD coupled cavity-cavity system is illustrated in Fig. 7. The QDs are represented by two ground states $|g\rangle$ and $|r\rangle$, where the state $|r\rangle$ is largely detuned with the respective cavity mode. The two ground states can be prepared via QD spin-states such as demonstrated remarkably in experiment in Ref. (Atatuer et al., 2006) with near-unity fidelity. The input weak photon pulse is assumed *h*-polarized, with an input pulse duration D (e.g. 1 ns) larger than the loaded cavity lifetime for the steady-state approximation. To remove the distinguishability of the two output photon spatial modes in the waveguide (transmitted and reflected), a reflecting element is inserted in the end of waveguide (such as a heterostructure interface), as shown in Fig. 7. This ensures that the photon always exits in the left-propagating mode $|L\rangle$ (from a right-propagating input mode $|R\rangle$) without any entanglement with the QD states. Alternatively, a Sagnac interferometer scheme such as introduced in Reference (Gao et al., 2008) can also be implemented to remove the spatial mode distinguishability and QD-photon entanglement. In this single input single output mode scheme, $|h\rangle$ and $|v\rangle$ represent the two polarization states of the input photon. We emphasize that in the below calculations we have considered the complete characteristics of the full system (including the end reflecting element and the resulting "standing wave" due to the long photon pulse width) where we examined the final left-propagating output mode $|L\rangle$ from a right-propagating input mode $|R\rangle$ (Fig. 7). The

reflection interference is included where we force $\hat{b}_{\text{in}}^{(2)} = \hat{b}_{\text{out}}^{(2)}$ (Fig. 4b) from the reflection element, when calculating the temporal pulse delays for the different QD states.

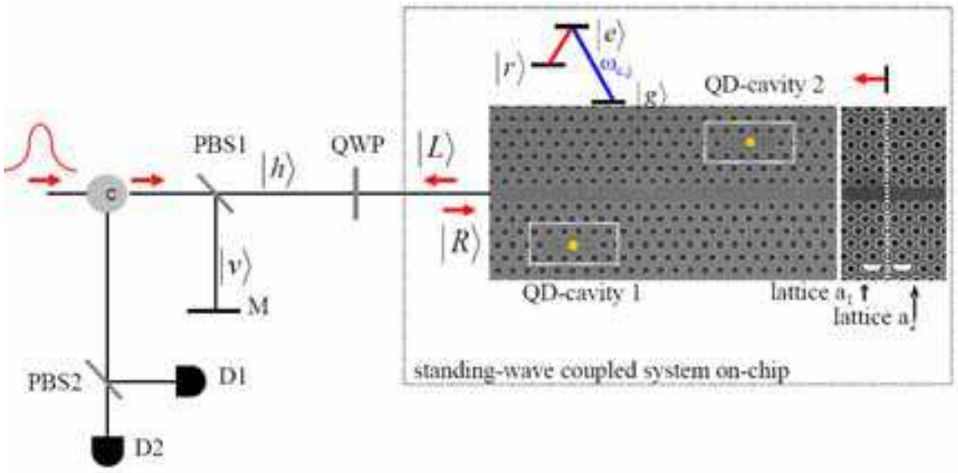

Fig. 7. Schematic to illustrate two-qubit quantum phase gate based on the coupled cavity-cavity multi-QD scheme. A heterostructure reflection element is introduced in the end of waveguide to remove spatial mode distinguishability, with only a single output mode $|L\rangle$ for an input photon mode $|R\rangle$. The QDs have a superposition of two ground states, $|g\rangle$ and $|r\rangle$. PBS1 and PBS2 represent the polarization beam splitters, D1 and D2 the single photon detectors, C the circulator, M the reflecting mirror. Here PBS1 and PBS2 are actually regarded as filters since only the h-polarized photon is required in our scheme. The response of detectors D1 and D2 provide an indication to show the gate operation success, and can also be used for measurement-induced entanglement in future.

To facilitate the discussion but without loss of generality, we describe the all resonance case (i.e., $\omega = \omega_{c(r),j}$) to describe the idea of the phase gate operation; in the subsequent numerical calculations, we will demonstrate the gate feasibility under non-ideal detunings. As an example, we focus on the realization of a two-qubit (two QDs) phase gate. Fig. 8 now shows the calculated reflection field (real and imaginary components) of the complete coupled cavity-cavity and two QD systems for the four superpositioned states $|\Psi\rangle_{\text{in}} = \alpha_1|r\rangle_1|r\rangle_2 + \alpha_2|g\rangle_1|r\rangle_2 + \alpha_3|r\rangle_1|g\rangle_2 + \alpha_4|g\rangle_1|g\rangle_2$. We address the following cases for the different QD states.

Case I: The two QDs are initially prepared in $|u\rangle_1|v\rangle_2$ ($u,v = g,r$) and at least one QD occupies the ground state $|r\rangle$. From Figs. 8a and 8b and for the all resonance case, we see that $\text{Re}[r_{21}] \simeq -1$ and $\text{Im}[r_{21}] \simeq 0$ under the over-coupling regime ($\kappa_0 \ll \kappa_1$) and with the large Purcell factor ($g^2/\Gamma\gamma \gg 1$). This fact can be understood by regarding the resonant condition ($\omega_{c,j} = \omega$). The input photon will be almost reflected by one *empty* cavity, in which the QD is in $|r\rangle$, resulting in a final state $|u\rangle_1|v\rangle_2|L\rangle$.

Case II: The QDs initially occupy in $|g\rangle_1|g\rangle_2$. In this case, note that the photon pulse interacts coherently with both cavities and two QDs, including the reflection element which is placed specifically to achieve $\hat{b}_{\text{in}}^{(2)} = \hat{b}_{\text{out}}^{(2)}$, before completely exiting the system. As demonstrated in Figs. 8a and 8b and for the all resonance case, the final output state is described by $\text{Re}[r_{21}] \simeq 1$ and $\text{Im}[r_{21}] \simeq 0$. The resulting state is $|g\rangle_1|g\rangle_2|L\rangle$. We note that the

photon loss is small for all four cases when the input photon pulse is on resonance with the cavity resonances, as can be done experimentally by tuning the input photon.

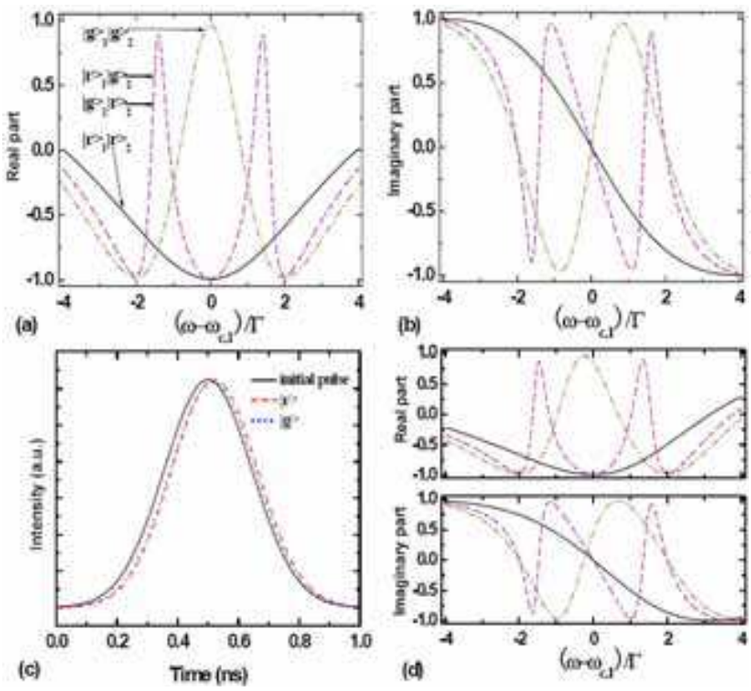

Fig. 8. Real (a) and imaginary (b) parts of the reflection coefficients for initial QD states, $|r\rangle_1|r\rangle_2$, $|r\rangle_1|g\rangle_2$, $|g\rangle_1|r\rangle_2$, and $|g\rangle_1|g\rangle_2$. Here we assume $|g_1(\vec{r})| = |g_2(\vec{r})| = 2\Gamma$, $\delta_{21} = \delta_1 = \delta_2 = 0$, and the propagation phase between the second cavity and the reflection element is adjusted as $\theta' = n\pi + \pi/2$ to compensate the phase shift induced by the mirror reflection (ideally, π). Other parameters are the same as Fig. 5a. (c) Shape function of the photon pulse for cases when the single QD is coupled ($|g\rangle$) or decoupled ($|r\rangle$) to the single cavity, and without the cavity. (d) Real and imaginary parts of the reflection coefficient when the reflection phase of the mirror deviates from ideal π with a deviation of 0.5.

Therefore, with the exit of the photon of the single input single output system, the state of the two QDs after the interaction is now described by $|\Psi\rangle_{\text{out}} = -\alpha_1|r\rangle_1|r\rangle_2 - \alpha_2|g\rangle_1|r\rangle_2 - \alpha_3|r\rangle_1|g\rangle_2 + \alpha_4|g\rangle_1|g\rangle_2$. Hence, after the above process and recombining at PBS1, the state of the QD-QD gate described by $U = e^{i\pi|g\rangle_{12}\langle g|}$ can be manipulated. Moreover, if $\alpha_i = 1/2 (i = 1,2,3,4)$, we have $|\Psi\rangle_{\text{out}} = (1/\sqrt{2})(|r\rangle_1|-\rangle_2 + |g\rangle_1|+\rangle_2)$ [where $|-\rangle_2 = 1/\sqrt{2}(|g\rangle_2 - |r\rangle_2)$ and $|+\rangle_2 = 1/\sqrt{2}(|g\rangle_2 + |r\rangle_2)$], which is the generation of the maximally entangled state in the coupled QDs. Most importantly, this idea can also be extended to realize an N-qubit gate with only one step, which is of importance for reducing the complexity of practical quantum computation and quantum algorithms for physical realization. In addition, using this configuration, some special entangled QD states (for e.g., the cluster state) can be generated (Cho and Lee, 2005).

We provide a few more notes on this designed coupled cavity-cavity multi-QD system. First, the temporal distinguishability is small for the single cavity-QD system, where in Fig. 8c we

plot the shape function of the output photon pulse for cases when the QD is coupled ($|g\rangle$), decoupled ($|r\rangle$), or without the cavity, through numerical simulation of the dynamical evolution of the system. The pulse shape function overlaps very well. Secondly, the calculated temporal distinguishability in the coherently coupled cavity-cavity multi-QD system is also small compared to the pulse duration D. Specifically, with the parameters in Fig. 8a, the photon delays due to the coupling to the cavities are calculated as approximately τ_{life}, $2\tau_{\text{life}}$, $2\tau_{\text{life}}$, and $4\tau_{\text{life}}$ in case of the states $|r\rangle_1|r\rangle_2$, $|r\rangle_1|g\rangle_2$, $|g\rangle_1|r\rangle_2$, and $|g\rangle_1|g\rangle_2$, respectively, where the loaded cavity τ_{life} is about 0.02 ns. The photon delay of the complete system is therefore sizably smaller than the pulse duration (of 1 ns, for example). Furthermore, this cavity-induced delay will furthermore decrease with increasing the coupling rate g, furthering reducing temporal distinguishability. Of course, the size of the chip is also small (tens of microns) so that the propagation time ($2S/v$, where S denotes the distance between the first cavity and the reflector, and v the group velocity) in the waveguide is much smaller than the pulse duration D. Thirdly, we examine the dependence of the overall system reflection coefficient on the phase variation from the reflection element, when deviating from the ideal π phase shift. Fig. 8d shows the numerical results, where a slight dependence is observed when there is a phase deviation of 0.5 from π. Moreover, the phase shift from the reflection element can be externally controlled stably, such as with an external and focused pump beam to thermally tune the reflection region.

3.4 Gate fidelity and photon loss

To exemplify the coupled cavity system, isolated single semiconductor QDs in high-Q small modal volume (V) photonic crystal cavities are potential candidates, such as self-assembled InAs QDs in GaAs cavities, or PbS nanocrystals in silicon cavities at near 1550 nm wavelengths. For PbS nanocrystal and silicon cavity material system, we use the following parameters in our calculations: $\gamma_s \sim 2$ MHz, $\gamma_p \sim 1$ GHz at cooled temperatures, $V \sim 4$ μm^3 at 1550 nm, with resulting single-photon coherent coupling rate $g \sim 12.4$ GHz. Loaded cavity Q in the range of 10^4 and 10^5 are achievable experimentally, with intrinsic Q up to 10^6 reported recently (Noda et al., 2007; Tanabe et al., 2007).

To characterize the present gate operation, Figs. 9a and 9b present the two-qubit phase gate fidelity F and photon losses P for various g and the parameters described above, even under non-ideal detuning conditions and the bad cavity limit. It should be noted here that, with δ_{21} and $\delta_{1,2}$, we can know the detuning between two QDs. For example, in case of $\delta_{21} = 5\kappa_0$ and $\delta_{1,2} = 0$, we deduce the detuning between the two QDs is $5\kappa_0$. Based on the above parameters, F can reach to 0.99 or more, and P can be below 0.04. As shown in Fig. 9, for cavity-cavity detunings in the range of the intrinsic cavity decay rate, both F and does not degrade significantly but is strongly dependent on the cavity decay rate. Likewise, with cavity-QD detuning that is comparable with the intrinsic cavity decay rate, both F and P does not change significantly but is dependent on the cavity decay rate. We note that the on-resonant photon loss P can be larger than the non-resonant case when g is small. This can be explained by considering the decay of QDs. When the QDs resonantly interact with cavity modes, the decay of QDs becomes distinct, resulting in an increasing of photon loss. Moreover, we note the QD-QD detuning plays an important role in the quantum gate

operations. Given the current large inhomogeneous distribution of QD transitions, however, active tuning methods such as Stark shifts would probably be needed to control the detuning within acceptable bounds to obtain strong quantum gate fidelity and low photon loss. Furthermore, we note that, with increasing *g*, the photon loss *P* exhibits an increase before a decrease, which can be understood by studying the photon loss when the QDs are in the state of $|g\rangle_1|g\rangle_2$. When $g \simeq \Gamma/2$, the absorption strength (resulting from κ_0 and γ) of the input photon by the coupled cavities reaches the maximum.

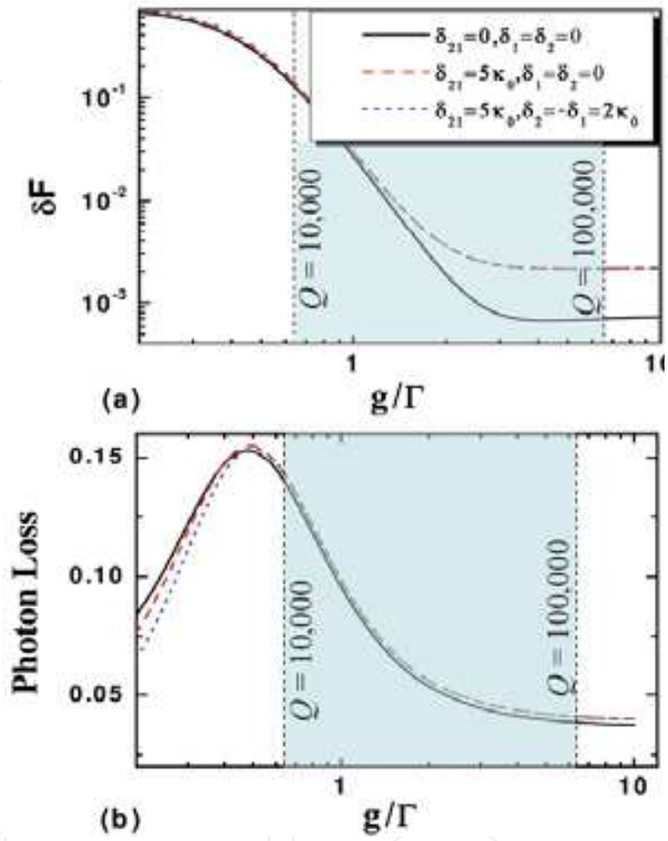

Fig. 9. Gate fidelity change ($\delta F \equiv 1 - F$) (a) and photon loss P (b) of the two-qubit gate versus g/Γ. The reflecting element has 95% reflectivity. Here the carrier frequency is assumed as $\varpi - 2.5\kappa_0$ to avoid the EIT-like peaks of two coupled empty cavities, and a scattering loss of 1% is used for the short propagation lengths. Other parameters are same as Fig. 6a. The shaded areas correspond to loaded cavity Q in the range of 10^4 to 10^5.

4. Summary

In this Chapter, with the nanocavities in photonic crystal, we theoretically introduce, derive, and demonstrate the robust implementation of a single spin-photon phase gate in a cavity-dipole-cavity system. The conditions of accidental degeneracy are examined to enforce complete transfer, either in the forward transmission or in reflection, of the qubit. In addition, we observe that a photon pulse is strikingly reflected by a cavity interacting with a single spin, even under the bad-cavity limit. This combined nanocrystal-cavity system,

examined in a silicon materials platform with lead chalcogenide nanocrystals in the near infrared, can serve as a QD spin-photon two-qubit quantum phase gate and, indeed, as a general quantum interface for large-array chip-based quantum information processing. To further utilize the high-Q and small-V nanocavities of photonic crystal, we also investigate the operation and performance of a scalable cavity–QD array on a photonic crystal chip towards controlled QD-QD quantum gates. The coupling among single-QD emitters and quantized cavity modes in a coherent array results in unique transmission spectra, with an optical analogue of EIT-like resonances providing potential photon manipulation. In the quantum phase gate operation, we note that the gate fidelity can reach 0.99 or more and the photon loss can be below 0.04 in a realistic semiconductor system, provided the non-ideal detunings are kept within the cavity decay rates. Our study provides a potential for a chip-scale quantum gate towards a potential quantum computing network with the platform of silicon photonic crystal.

For future experimental quantum information processing in photonic crystal, we note that it is possible to realize the initial idea in a single nanocavity-QD coupled system, as experimentally demonstrated in the context of strong cavity-QD coupling (Hennessy et al., 2007; Badolato et al., 2006; Reithmaier et al., 2004; Yoshie et al., 2004; Faraon et al., 2008; Fushman et al., 2008) and the quantum state transfer between a single QD and a target cavity (Englund et al., 2007a). This opens the door to construct the basic building blocks for future chip-based quantum information processing systems. However, it is still a challenge to implement quantum information with a nanocavity array in photonic crystal. The challenge includes several main technique difficulties. First, it is necessary to precisely place a single two-level nanocrystal (or other QDs) with respect to the corresponding nanocavity mode in photonic crystal, for the largest Rabi frequency, and also to position across an array. Second, both the cavity resonances and QD transitions should spectrally overlap within approximately the cavity or exciton linewidths, although our theoretical model is still robust with small QD-QD, cavity-QD, and cavity-cavity detunings. The former challenge depends on careful nanofabrication techniques, while the latter condition can be relaxed through high-precision tunability of the cavity resonances or QD transitions. Moreover, we note that the ultrahigh-Q and low-V regime is desired to operate well into the strong coupling regime, suppressed chip-scale photon losses or improved collection to improve quantum state transfer, as well as control of dephasing especially at high temperatures in order for chip-level scalability in solid-state quantum information nanosciences.

5. References

Angelakis, D. G.; Santos, M. F. & Bose, S. (2007). Photon-blockade-induced Mott transitions and XY spin models in coupled cavity arrays. *Physical Review A*, Vol. 76, No. 3, 031805.

Asano, T.; Song, B.-S. & Noda, S. (2006). Analysis of the experimental Q factors (~1 million) of photonic crystal nanocavities. *Optics Express*, Vol. 14, No. 5, 1996-2002.

Atatüre, M.; Dreiser, J.; Badolato, A.; Högele, A.; Karrai, K. & Imamoglu, A. (2006). Quantum-dot spin-state preparation with near-unity fidelity. *Science*, Vol. 312, No. 5773, 551-553.

Badolato, A.; Hennessy, K.; Atatüre, M.; Dreiser, J. Hu, E.; Petroff, P. M. & Imamoglu, A. (2005). Deterministic coupling of single quantum dots to single nanocavity modes. *Science*, Vol. 308, No. 5725, 1158-1161.

BarWicz, T.; Watts, M. R.; Popović, M. A.; Rakich, P. T.; Socci, L.; Kärtner, F. X.; Ippen, E. P. & Smith, H. I. (2007). Polarization-transparent microphotonic devices in the strong confinement limit. *Nature Photonics*, Vol. 1, No. 1, 57-60.

Bose, R.; Yang, X.-D.; Chatterjee, R.; Gao, J. & Wong, C.-W. (2007). Weak coupling interactions of colloidal lead sulphide nanocrystals with silicon photonic crystal nanocavities near 1.55 mu m at room temperature. *Applied Physics Letters*, Vol. 90, No. 11, 111117.

Brattke, S.; Varcoe, B. T. H. & Walther, H. (2001). Generation of Photon Number States on Demand via Cavity Quantum Electrodynamics. *Physical Review Letters*, Vol 86, No. 16, 3534-4537.

Brune, M.; Hagley, E.; Dreyer, J.; Maitre, X.; Maali, A.; Wunderlich, C.; Raimond, J. M. & Haroche, S. (1996). Observing the Progressive Decoherence of the "Meter" in a Quantum Measurement. *Physical Review Letters*, Vol 77, No. 24, 4887-4890.

Cabrillo, C.; Cirac, J. I.; Garcia-Fernandez, P. & Zoller, P. (1999). Creation of entangled states of distant atoms by interference. *Physical Review A*, Vol 59, No.2, 1025-1033.

Cirac, J. I.; Zoller, P.; Kimble, H. J. & Mabuchi, H. (1997). Quantum state transfer and entanglement distribution among distant nodes in a quantum network. *Physical Review A*, Vol. 78, No. 16, 3221-3224.

Cho, J. & Lee, H.–W. (2005). Generation of atomic cluster states through the cavity input-output process. *Physical Review Letters*, Vol. 95, No. 16, 160501.

Duan, L.-M.; Kuzmich, A. & Kimble, H. J. (2003). Cavity QED and quantum-information processing with "hot" trapped atoms. *Physical Review A* Vol. 67, No. 3, 032305.

Duan, L.-M. & Kimble, H. J. (2004). Scalable photonic quantum computation through cavity-assisted interactions. *Physical Review Letters*, Vol. 92, No. 12, 127902.

Englund, D.; Faraon, A.; Fushman, I.; Stoltz, N.; Petroff, P. & Vuckovic, J. (2007a). Controlling cavity reflectivity with a single quantum dot. *Nature*, Vol. 450, 857-861.

Gao, J.; Sun, F.–W. & Wong, C.-W. (2008). Implementation scheme for quantum controlled phase-flip gate through quantum dot in slow-light photonic crystal waveguide. *Applied Physics Letters*, Vol. 93, (2008) 151108.

Fan, S.; Villeneuve, P. R.; Joannopoulos, J. D. & Haus, H. A. (1998). Channel drop tunneling through localized states. *Physical Review Letters*, Vol. 80, No. 5, 960-963.

Faraon, A.; Fushman, I.; Englund, D.; Stoltz, N.; Petroff, P. & Vuckovic, J. (2008). Coherent generation of nonclassical light on a chip via photon-induced tunneling and blockade. *Nature Physics*, Vol 4, 859-863.

Fleischhauer, M.; Imamoglu, A. & Marangos, J. P. (2005). Electromagnetically induced transparency: Optics in coherent media. *Reviews of Modern Physics*, Vol. 77, No. 2, 633-673.

Foresi, J. S.; Villeneuve, P. R.; Ferrera, J.; Thoen, E. R.; Steinmeyer, G.; Fan, S.; Joannopoulos, J. D.; Kimerling, L. C.; Smith, H. I. & Ippen, E. P. (1997). Photonic-bandgap microcavities in optical waveguides. *Nature*, Vol. 390, 143-145.

Fushman, I.; Englund, D. & Vučković, J. (2005). Coupling of PbS quantum dots to photonic crystal cavities at room temperature. *Applied Physics Letters*, Vol. 87, No. 24, 241102.

Fushman, I.; Englund, D.; Faraon, A.; Stoltz, N.; Petroff, P. & Vuckovic, J. (2008). Controlled Phase Shifts with a Single Quantum Dot, Science, Vol 320, No. 5877, 769-772.

Guo, L.; Krauss, T. D.; Poitras, C. B.; Lipson, M.; Teng, X. & Yang, H. (2006). Energy transfer between colloidal semiconductor nanocrystals in an optical microcavity. *Applied Physics Letters*, Vol. 89, No. 6, 061104.

Greentree, A. D.; Tahan, C.; Cole, J. H. & Hollenberg, L. C. L. (2006). Quantum phase transitions of light. *Nature Physics*, Vol. 2, 856-861.

Hartmann, M. J.; Brandão, F. G. S. L. & Plenio M. B. (2006). Strong interacting polaritons in coupled arrays of cavities. *Nature Physics*, Vol. 2, 849-855.

Hartmann, M. J. & Plenio M. B. (2007). Strong photon nonlinearities and photonic Mott insulators. *Phys. Rev. Lett.*, Vol. 99, No. 10, 103601.

Hartmann, M. J.; Brandão, F. G. S. L. & Plenio, M. B. (2007). Effective spin systems in coupled microcavities. *Physical Review Letters*, Vol. 99, No. 16, 160501.

Hennessy, K.; Badolato, A.; Winger, M.; Gerace, D.; Atatüre, M.; Gulde, S.; Fält, S.; Hu, E. L. & Imamoglu, A. (2007). Quantum nature of a strongly coupled single quantum dot-cavity System. *Nature*, Vol. 445, 896-899.

Hughes, S. (2007). Coupled-cavity QED using planar photonic crystals. *Physical Review Letters*, Vol. 98, No. 8, 083603.

Khitrova, G.; Gibbs, H. M.; Kira, M.; Koch, S. W. & Scherer, A. (2006). Vacuum Rabi splitting in semiconductors. *Nature Physics*, Vol. 2, No. 81, 81-90.

Law, C. K. & Eberly, J. H. (1996). Arbitrary Control of a Quantum Electromagnetic Field. *Physical Review Letters*, Vol. 76, No. 7, 1055-1058.

Mabuchi, H. & Doherty, A. C. (2002). Cavity quantum electrodynamics: coherence in context. *Science* Vol. 298, No. 5597, 1372-1377.

Min, B.-K.; Kim, J.-E. & Park, H. Y. (2004). Channel drop filters using resonant tunneling processes in two-dimensional triangular lattice photonic crystal slabs. *Optics Communications*, Vol. 273, No. 1-3, 59-63.

Noda, S.; Fujita, M. & Asano, T. (2007). Spontaneous-emission control by photonic crystals and nanocavities. *Nature Photonics*, Vol. 1, 449-458.

Pachos, J. & Walther, H. (2002). Quantum Computation with Trapped Ions in an Optical Cavity. *Physical Review Letters*, Vol 89, No. 18, 187903.

Parkins, A. S.; Marte, P.; Zoller, P. & Kimble, H. J. (1993). Synthesis of arbitrary quantum states via adiabatic transfer of Zeeman coherence. *Physical Review Letters*, Vol. 71, No. 19, 3095-3098.

Pellizzari, T.; Gardiner, S. A.; Cirac, J. I. & P. Zoller (1995). Decoherence, Continuous Observation, and Quantum Computing: A Cavity QED Model. *Physical Review Letters*, Vol 75, No. 21, 3788-3791.

Reithmaier, J. P.; SJk, G.; Löffler, A.; Hofmann, C.; Kuhn, S.; Reitzenstein, S.; Keldysh, L. V.; Kulakovskii, V. D.; Reinecke, T. L. & Forchel, A. (2004). Strong coupling in a single quantum dot-semiconductor microcavity system. *Nature*, Vol. 432, No. 7014, 197-200.

Santos, M. F. (2005). Universal and Deterministic Manipulation of the Quantum State of Harmonic Oscillators: A Route to Unitary Gates for Fock State Qubits. *Physical Review Letters*, Vol. 95, No. 1, 010504.

Smith, D.; Chang, H.; Fuller, K. A.; Rosenberger, A. T. & Boyd, R. W. (2004). Coupled-resonator-induced transparency. *Physical Review A*, Vol. 69, No. 6, 063804.

Srinivasan, K. & Painter, O. (2007). Mode coupling and cavity-quantum-dot interactions in a fiber-coupled microdisk cavity. *Physical Review A*, Vol. 75, No. 2, 023814.

Sørensen, A. S. & Mølmer, K. (2003). Measurement induced entanglement and quantum computation with atoms in optical cavities. *Physical Review Letters*, Vol. 91, No. 9, 097905.

Tanabe, T.; Notomi, M.; Kuramochi, E.; Shinya, A. & Taniyama, H. (2006). Trapping and delaying photons for one nanosecond in an ultrasmall high-Q photonic-crystal nanocavity. *Nature Photonics*, Vol. 1, 49-52.

Tosuka, K.; Kobayashi, N.; Tomita, M. (2007). Slow light in coupled-resonator-induced transparency. *Physical Review Letters*, Vol. 98, No. 21, 213904.

Vahala, H. J. (2004). Optical cavities. *Nature*, Vol 424, No. 7253, 839-846.

Vogel, K.; Akulin, V. M. & Schleich, W. P. (1993). Quantum state engineering of the radiation field. *Physical Review Letters*, Vol. 71, No. 12, 1816-1819.

Waks, E. & Vuckvic, J. (2006). Dispersive properties and large Kerr nonlinearities using dipole-induced transparency in a single-sided cavity. *Physical Review A.*, Vol. 73, No. 4, 041803.

Xiao, X.-F.; Han, Z.-F. & Guo G.-C. (2006). Quantum computation without strict strong coupling on a silicon chip. *Physical Review A*, Vol. 73, No. 5, 052324.

Xiao, Y.-F.; Gao, J.; Yang, X.; Bose, R. & Guo, G.-C. (2007a). Nanocrystals in silicon photonic crystal standing-wave cavities as spin-photon phase gates for quantum information processing. *Applied Physics Letters*, Vol. 91, 151105.

Xiao, Y.-F.; Zou, X.-B.; Jiang, W.; Chen, Y.-L. & Guo, G.-C. (2007b). Analog to multiple electromagnetically induced transparency in all-optical drop-filter systems. *Physical Review A*, Vol. 75, No. 6, 063833.

Xiao, Y.-F.; Gao, J.; Zou, X.-B.; McMillan, J.-F.; Yang, X.; Chen, Y.-L.; Han, Z.-F.; Guo, G.-C. & Wong, C. W. (2008). Coupled quantum electrodynamics in photonic crystal cavities towards controlled phase gate operations. *New Journal of Physics*, Vol. 10, 123013.

Xu, Q.; Sandhu, S.; Povinelli, M. L.; Shakya, J.; Fan, S. & Lipson, M. (2006). Experimental Realization of an on-chip all-optical analogue to electromagnetically induced transparency. *Physical Review Letters*, Vol. 96, No. 12, 123901.

Xu, Q.; Dong, P. & Lipson, M. (2007). Breaking the delay-bandwidth limit in a photonic structure. *Nature Physics*, Vol. 3, 406-410.

Xu, Y.; Li, Y.; Lee, R. K. & Yariv, A. (2000). Scattering-theory analysis of waveguide-resonator coupling. *Physical Review E*, Vol. 62, No. 5, 7389-7404

Yanik, M. F.; Suh, W.; Wang, Z. & Fan, S. (2004). Stopping light in a waveguide with an all-optical analog of electromagnetically induced transparency. *Physical Review Letters*, Vol. 93, No. 23, 233903.

Yoshie, T.; Scherer, A.; Hendrickson, J.; Khitrova, G.; Gibbs, H. M.; Rupper, G.; Ell, C.; Shchekin, O. B. & Deppe, D. G. (2004). Vacuum Rabi splitting with a single quantum dot in a photonic crystal nanocavity. *Nature*, Vol. 432, 200-203.

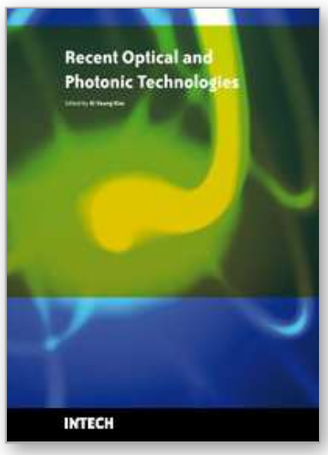

Recent Optical and Photonic Technologies

Edited by Ki Young Kim

ISBN 978-953-7619-71-8
Hard cover, 450 pages
Publisher InTech
Published online 01, January, 2010
Published in print edition January, 2010

Research and development in modern optical and photonic technologies have witnessed quite fast growing advancements in various fundamental and application areas due to availability of novel fabrication and measurement techniques, advanced numerical simulation tools and methods, as well as due to the increasing practical demands. The recent advancements have also been accompanied by the appearance of various interdisciplinary topics. The book attempts to put together state-of-the-art research and development in optical and photonic technologies. It consists of 21 chapters that focus on interesting four topics of photonic crystals (first 5 chapters), THz techniques and applications (next 7 chapters), nanoscale optical techniques and applications (next 5 chapters), and optical trapping and manipulation (last 4 chapters), in which a fundamental theory, numerical simulation techniques, measurement techniques and methods, and various application examples are considered. This book deals with recent and advanced research results and comprehensive reviews on optical and photonic technologies covering the aforementioned topics. I believe that the advanced techniques and research described here may also be applicable to other contemporary research areas in optical and photonic technologies. Thus, I hope the readers will be inspired to start or to improve further their own research and technologies and to expand potential applications. I would like to express my sincere gratitude to all the authors for their outstanding contributions to this book.

INTECH
open science | open minds

InTech Europe
University Campus STeP Ri
Slavka Krautzeka 83/A
51000 Rijeka, Croatia
Phone: +385 (51) 770 447

InTech China
Unit 405, Office Block, Hotel Equatorial Shanghai
No.65, Yan An Road (West), Shanghai, 200040, China
中国上海市延安西路65号上海国际贵都大饭店办公楼405单元
Phone: +86-21-62489820

Fax: +385 (51) 686 166
www.intechopen.com

Fax: +86-21-62489821

IntechOpen